Four New Lead(II) Thiolate Cluster Complexes – Unexpected Products of a Conventional Synthesis

Andreas Eichhöfer*[a]

Keywords: Cluster compounds / Lead / Sulfur / UV/Vis spectroscopy

The reaction of $Pb(OOCCH_3)_2 \cdot 3H_2O$ with 2.1 equiv. of HS-2,6-$(CH_3)_2C_6H_3$ in ethanol/water is expected to give [Pb{S-2,6-$(CH_3)_2C_6H_3$}$_2$]. However, we obtained an orange powder whose elemental analysis disagrees with that of the expected product and indicates small amounts of oxygen. Layering of concentrated solutions of this orange powder in dry THF with pentane under nitrogen results in the formation of a mixture of three identifiable crystalline compounds, namely [Pb_{10}{S-2,6-$(CH_3)_2C_6H_3$}$_{20}$], [Pb_6S{S-2,6-$(CH_3)_2C_6H_3$}$_{10}(C_4H_8O)_4$] and [Pb_8O_2{S-2,6-$(CH_3)_2C_6H_3$}$_{12}$]. In contrast, fractional crystallization from dilute solutions initially yielded only yellow crystals of [$Pb_{14}O_6${S-2,6-$(CH_3)_2C_6H_3$}$_{16}$]. Further concentration of the supernatant solution yielded, upon layering with pentane, [Pb_6S{S-2,6-$(CH_3)_2C_6H_3$}$_{10}(C_4H_8O)_4$] and [Pb_{10}{S-2,6-$(CH_3)_2C_6H_3$}$_{20}$], which are almost completely separable by controlling the duration of the crystallization step and the amount of condensed pentane. Recrystallization of the crude orange powder under aerobic conditions produces pure [$Pb_{14}O_6${S-2,6-$(CH_3)_2C_6H_3$}$_{16}$] with a yield five times higher than that under nitrogen. This shows that it is sensitive to oxidation by oxygen in solution. The structures of all four complexes have been determined by single-crystal X-ray analysis. The net formed by the six oxygen and twelve lead atoms in the center of [$Pb_{14}O_6${S-2,6-$(CH_3)_2C_6H_3$}$_{16}$] resembles a small piece of a layer of the solid-state structure of red PbO.

Introduction

Lead chalcogenide nanocrystals (PbS, PbSe, PbTe) have recently attracted interest due to their unique properties.[1–3] Size-quantization effects are strongly pronounced in these materials because of their relatively large exciton Bohr radii. Furthermore, the quantum size effect offers potential photonic applications. Theoretically, PbSe nanocrystals (NCs) are predicted to have absorptive and dispersive nonlinearities 1000 times larger than those of CdSe NCs of the same size.[4] However, in contrast to the recent, distinct growth in the chemistry of transition metal chalcogenide clusters,[5,6] related polynuclear molecules of the heavier main group elements seem to be rather unexplored to date.[7] It is known that the reaction of lead thiolates of the general formula $Pb(SR)_2$ (R = organic group) with stoichiometric amounts of sulfur or selenium yields the corresponding lead chalcogenides.[8] These findings suggest that nonstoichiometric reactions could probably lead to metastable lead chalcogenolato/chalcogenide cluster molecules. Therefore, we became interested in the synthesis of lead thiolate complexes as starting materials for the synthesis of such cluster molecules. In order to avoid known solubility problems of the mostly polymeric lead thiolates[8–10] we followed a recent recommendation of Briand[11] concerning the use of 2,6-dimethylthiophenol, which was reported to yield soluble [Pb{S-2,6-$(CH_3)_2C_6H_3$}$_2$]. However, the direct reaction of $Pb(OOCCH_3)_2 \cdot 3H_2O$ with 2.1 equiv. of HS-2,6-$(CH_3)_2C_6H_3$ at 60 °C obviously leads not only to the expected product [Pb{S-2,6-$(CH_3)_2C_6H_3$}$_2$] but also yields lead thiolate cluster complexes which have sulfur or oxygen atoms incorporated in the cluster framework, the structures of which are reported here.

Results and Discussion

In order to synthesize [Pb{S-2,6-$(CH_3)_2C_6H_3$}$_2$] we used the method of Shaw and Woods developed for the synthesis of [Pb(S-2-$CH_3C_6H_4$)$_2$].[8] The reaction of $Pb(OOCCH_3)_2 \cdot 3H_2O$ with 2.1 equiv. of HS-2,6-$(CH_3)_2C_6H_3$ in aqueous ethanol at 60 °C yielded an orange-red precipitate, which was filtered and dried. The elemental analysis disagrees with the expected product [Pb{S-2,6-$(CH_3)_2C_6H_3$}$_2$] especially with respect to the low amount of sulfur, a fact which has also been observed by Shaw et al. in the related synthesis of some other lead thiolate complexes. Additionally, the presence of small amounts of oxygen is indicated by the analysis. Layering of concentrated solutions of the crude product in dried THF with pentane results in the formation of a mixture of the crystalline compounds **1**–**3**, which could be identified by single-crystal X-ray analysis. In contrast to this, a solution 1/5 as concentrated in dried THF led to the crystallization of small amounts of **4** (12% calculated for

[a] Institut für Nanotechnologie, Forschungszentrum Karlsruhe, Postfach 3640, 76021 Karlsruhe, Germany
Fax: +49-7247-82-6368
E-mail: eichhoefer@int.fzk.de

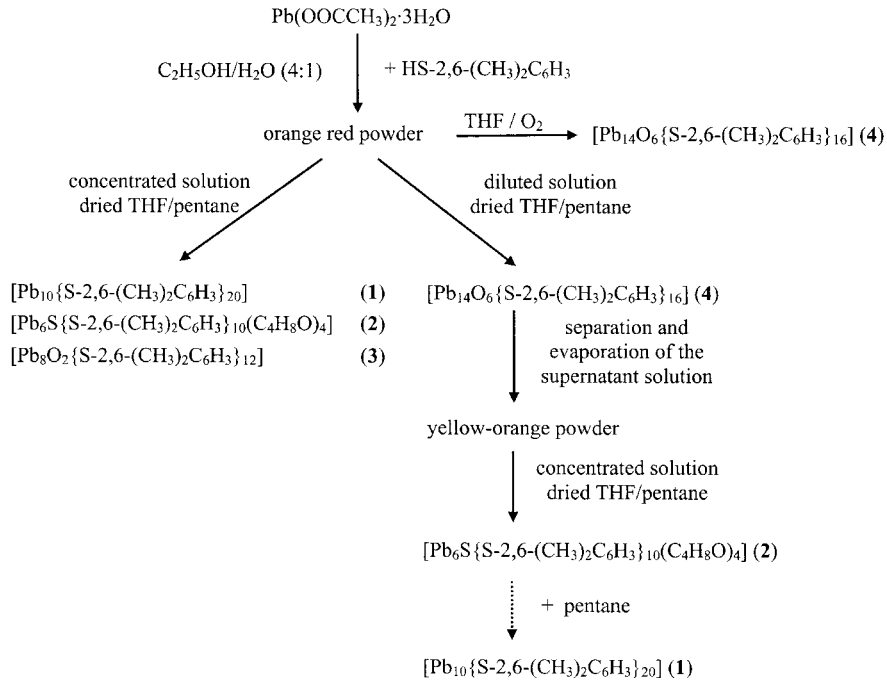

Pb) as the only product. Evaporation of the solvents of the clear supernatant yellow solution in vacuo produced a yellow-orange powder which was redissolved in 10 mL of THF. Layering of this concentrated solution with pentane yielded, firstly, crystals of **2**, followed by crystals of **1**, without any crystals of either **3** or **4**.

Obviously, the oxygen present in the crude orange powder was in this way completely bound by **4** and thus removed from the reaction solution. However, the crystallization of **1** and **2** proceeds in such a way that, initially, orange plate-like crystals of **2** appear, which tend to form solidified droplets of crystalline material after the layering process, while bundles of light-orange needles of **1** start to grow a few days later at higher concentrations of pentane. In this way, **1** and **2** can be nearly completely separated, as shown by powder diffraction patterns and elemental analysis (see below). The yield of **4** could be increased up to 56% by performing the recrystallization under aerobic conditions, which shows that the crude orange powder is sensitive to oxidation by oxygen in solution.

The light-orange, plate-like needles were found to display the desired composition $[Pb\{S\text{-}2,6\text{-}(CH_3)_2C_6H_3\}_2]$. Interestingly, the structure is neither polymeric, as in $[Pb(SC_6H_5)_2]_n$[9] or $[Pb(S\text{-}4\text{-}CH_3C_6H_4)_2]_n$,[10] nor trimeric, as in $[Pb_3(S\text{-}2,6\text{-}i C_3H_7C_6H_3)_6]$,[12] but is found to be oligomeric $[Pb_{10}\{S\text{-}2,6\text{-}(CH_3)_2C_6H_3\}_{20}]$ (**1**). Complex **1** crystallizes in the space group *Pbcn* with the molecule residing on an inversion center (Figure 1). The Pb–S contacts in the range of 255.8–317.5 pm have been assigned as bonds (solid lines), similar to those observed in the lead thiolates mentioned above, while longer contacts have been drawn for all molecules as dashed lines. Contacts to the next molecular unit are larger than 500 pm, which proves the oligomeric character of **1**. The lead atoms exhibit different coordination modes. Pb(2), and Pb(4) are in a distorted tetrahedral geometry comprising three sulfur atoms and the stereochemically active inert electron pair, whilst Pb(3) is bonded to six sulfur atoms in a highly distorted octahedral geometry caused by the additional inert electron pair. Pb(1) and Pb(5) possess complex coordination environments comprised of either five or four sulfur atoms. A comparison of the measured and calculated powder diffraction pattern of **1** (Figure 2) reveals the crystalline purity of the product isolated by fractional crystallization, as mentioned above.

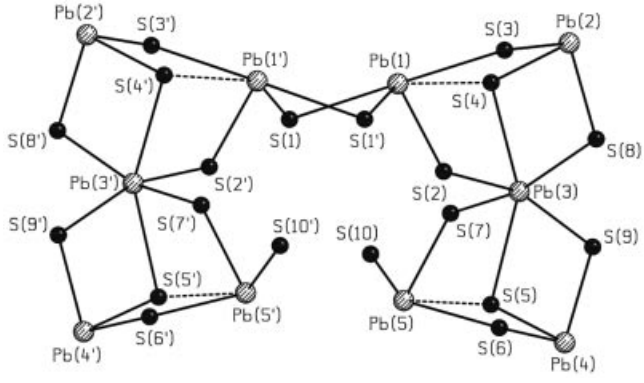

Figure 1. Molecular structure of $[Pb_{10}\{S\text{-}2,6\text{-}(CH_3)_2C_6H_3\}_{20}]$ (**1**). C and H atoms omitted for clarity. Selected bond lengths [pm] (solid lines): Pb(1)–S(2) 265.4(4), Pb(1)–S(1′) 269.1(4), Pb(1)–S(1) 298.1(4), Pb(1)–S(3) 305.9(5), Pb(2)–S(8) 265.8(4), Pb(2)–S(3) 267.9(5), Pb(2)–S(4) 275.4(3), Pb(3)–S(7) 2788(4), Pb(3)–S(2) 280.1(4), Pb(3)–S(4) 293.6(3), Pb(3)–S(5) 303.4(3), Pb(3)–S(8) 313.1(4), Pb(3)–S(9) 317.5(4), Pb(4)–S(9) 263.3(4), Pb(4)–S(5) 272.5(4), Pb(4)–S(6) 275.0(4), Pb(5)–S(10) 255.8(5), Pb(5)–S(7) 266.4(4), Pb(5)–S(6) 278.9(5). Weak contacts [pm] (dashed lines): Pb(5)–S(5) 355.5, Pb(1)–S(4) 362.7. Symmetry transformation for generation of equivalent atoms: $-x, y, -z + 0.5$.

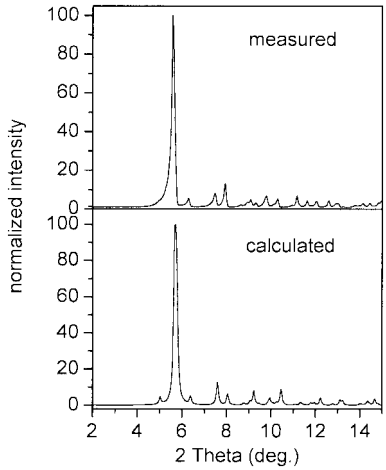

Figure 2. Measured (top) and calculated (bottom) powder diffraction pattern of $[Pb_{10}\{S\text{-}2,6\text{-}(CH_3)_2C_6H_3\}_{20}]$ (**1**).

The orange hexagonally shaped plates that form solidified droplets of crystalline material after the layering process were characterized to be $[Pb_6S\{S\text{-}2,6\text{-}(CH_3)_2C_6H_3\}_{10}(C_4H_8O)_4]$ (**2**). Obviously, part of the precursor thiol undergoes cleavage of the S–Aryl bond under the given experimental conditions. Complex **2** crystallizes in the $P\bar{1}$ space group with the central sulfur atom occupying an inversion center (Figure 3). The six lead atoms form an elongated octahedron whose eight trigonal faces are bridged by sulfur atoms, with Pb–S contacts mapped as bonds ranging from 262.7(2) to 311.3(3) pm. The two "axial" lead atoms [Pb(1) and Pb(1′)] are each additionally bonded to a thiolate ligand, while the equatorial lead atoms [Pb(2), Pb(2′), Pb(3), and Pb(3′)] are weakly coordinated by a THF solvent molecule (Pb–O: 300.2–304.2 pm). This leads to an octahedral coordination geometry for Pb(2), Pb(2′), Pb(3) and Pb(3′) which is distorted by the inert electron pair. Pb(1) and Pb(1′) are bonded to the five nearest sulfur atoms [S(2)–S(5) and symmetry-equivalent atoms] in a distorted square-pyramidal fashion with additional weak coordination by S(1) from the bottom face [Pb(1)–S(1): 350.6 pm]. Again, a comparison of the measured and calculated powder diffraction pattern of **2** (Figure 4) reveals the crystalline purity of the product that was isolated by fractional crystallization, as mentioned above.

Yellow, triclinic-shaped blocks were identified as the mixed lead oxide thiolate cluster complex $[Pb_8O_2\{SC_6H_3(CH_3)_2\}_{12}]$ (**3**). This is even observed when using freshly dried and distilled THF which suggests that Pb–O units are already present in the crude orange powder, a fact which was additionally supported by elemental analysis. The molecular structure of **3** ($\bar{1}$ symmetry), which crystallizes in the $P\bar{1}$ space group, consists of an octanuclear lead thiolate cluster which additionally incorporates two oxygen atoms (Figure 5). The two Pb_3O units are nearly planar [deviation of O(1) from the trigonal plane is 44 pm] with an average of 220.9(2) pm for the Pb–O distances. A similar structural unit is found in the pentanuclear, oxygen-centered lead thiolate cluster $[Pb_5O\{S\text{-}2,4,6\text{-}(CF_3)_3C_6H_2\}_8]\cdot 2C_7H_8$.[13] An additional "PbS-2,6-$(CH_3)_2C_6H_3$" unit is bonded to these two trigonal faces through three thiolate ligands [S(1), S(3), S(4), and equivalent atoms] forming two mixed oxide/thiolate-bridged Pb_4OS_5 cluster units which are linked at their Pb_3O faces by four additional μ_3-thiolate ligands [S(2), S(2′), S(5), and S(5′)]. The Pb–S distances are in the range of 256.2(3)/310.0(3) pm with eight additional weaker and longer contacts between 334.9 pm [Pb(2)–S(5)] and 361.4 pm [Pb(4)–S(4)].

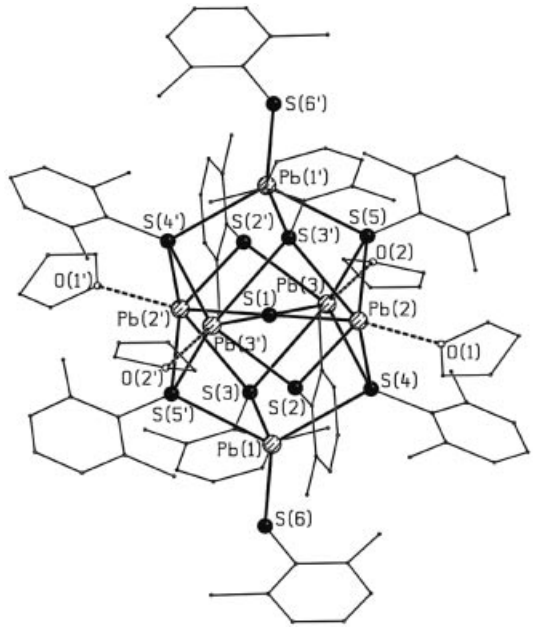

Figure 3. Molecular structure of $[Pb_6S\{S\text{-}2,6\text{-}(CH_3)_2C_6H_3\}_{10}(C_4H_8O)_4]$ (**2**). C and H atoms omitted for clarity. Selected bond lengths [pm] (solid lines): Pb(1)–S(6) 262.7(2), Pb(1)–S(3) 266.4(3), Pb(1)–S(4) 307.6(2), Pb(2)–S(4) 280.6(2), Pb(2)–S(2) 281.8(2), Pb(2)–S(1) 283.5(2), Pb(2)–S(3′) 309.3(2), Pb(2)–S(5) 312.1(2), Pb(3)–S(5) 276.0(2), Pb(3)–S(1) 283.36(8), Pb(3)–S(2′) 284.0(3), Pb(3)–S(4) 311.3(3). Weak contacts [pm] (dashed lines): Pb(1)–S(1) 350.6, Pb(1)–S(2) 353.6, Pb(2)–O(1) 304.1(3), Pb(3)–O(2) 300.2(3). Symmetry transformation for generation of equivalent atoms: $-x + 1, -y + 2, -z + 1$.

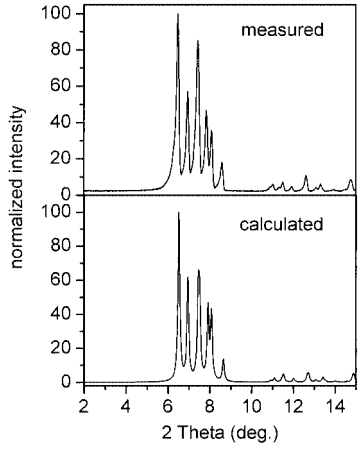

Figure 4. Measured (top) and calculated (bottom) powder diffraction pattern of $[Pb_6S\{S\text{-}2,6\text{-}(CH_3)_2C_6H_3\}_{10}(C_4H_8O)_4]$ (**2**).

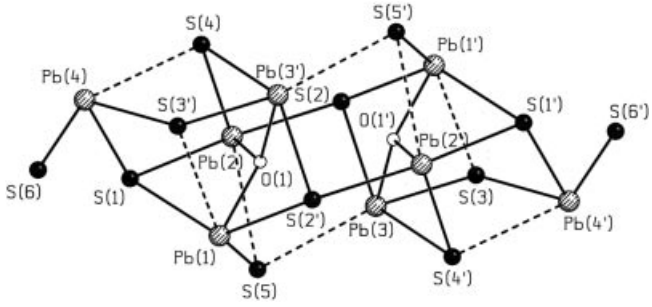

Figure 5. Molecular structure of $[Pb_8O_2\{S\text{-}2,6\text{-}(CH_3)_2C_6H_3\}_{12}]$ (**3**). C and H atoms omitted for clarity. Selected bond lengths [pm] (solid lines): Pb(1)–O(1) 220.5(6), Pb(2)–O(1) 222.4(6) Pb(3)–O(1′) 219.8(7), Pb(1)–S(5) 269.4(3), Pb(1)–S(1) 289.4(3), Pb(2)–S(4) 276.9(3), Pb(2)–S(2) 282.0(3), Pb(2)–S(1) 310.0(3), Pb(3)–S(3) 279.3(3), Pb(3)–S(2) 300.4(4), Pb(3)–S(4′) 302.6(4), Pb(4)–S(6) 256.2(3), Pb(4)–S(3′) 273.8(4), Pb(4)–S(1) 275.8(3). Weak contacts [pm] (dashed lines): Pb(1)–S(3′) 337.5, Pb(2)–S(5) 334.9, Pb(3)–S(5) 342.3, Pb(4)–S(4) 361.4. Symmetry transformation for generation of equivalent atoms: $-x$, $-y + 1$, $-z + 1$.

Small, yellow, needle-like plates of $[Pb_{14}O_6\{SC_6H_3\text{-}(CH_3)_2\}_{16}]$ (**4**) were found to be the only product crystallizing from dilute solutions of the crude orange-red powder in THF. Again, the use of freshly dried and distilled THF suggests that the oxygen can, in principle, only originate from compounds with Pb–O units that are already present in the crude powder. Interestingly, the yield of **4** is considerably increased upon dissolution of the crude powder in THF under aerobic conditions, which suggests that **4** can be seen as a stable oxidation product of the crude orange powder. This is in agreement with the investigations of Edelmann et al., who found $[Pb_5O\{S\text{-}2,4,6\text{-}(CF_3)_3C_6H_2\}_8]\cdot 2C_7H_8$ to be an oxidation product of the lead(II) thiolate $[Pb\{S\text{-}2,4,6\text{-}(CF_3)_3C_6H_2\}_2]$.[13] Complex **4** crystallizes in the $P\bar{1}$ space group and exhibits $\bar{1}$ symmetry (Figure 6). The net formed by the six oxygen [O(1), O(2), O(3), and symmetry-equivalent atoms] and twelve of the lead atoms [Pb(1)–Pb(6) and symmetry-equivalent atoms] resembles a small piece of a layer of the solid-state structure of red PbO, every layer of which is composed of a quadratic packing of oxygen atoms with the lead atoms occupying the quadratic cavities alternately above and below the oxygen planes. The Pb–O distances, with an average of 233.5 pm, are slightly longer in **4** than those in the red form of PbO (230 pm).[14] However, twenty of the contacts lie within a narrow range of 221.5–232.0(10) pm while four distances, namely Pb(2)–O(1′) [242.1(10) pm], Pb(2)–O(2) [269.6(10) pm], and distances to symmetry-equivalent atoms, show significantly larger values. The 16 thiolate ligands additionally bridge the lead atoms in different coordination modes, including the two remaining lead atoms Pb(7) and Pb(7′). The Pb–S bonds have been mapped in Figure 6 and range from 262.7(6) to 315.0(6) pm. A comparison of the measured X-ray powder patterns of a suspension of **4** in the mother liquor with the calculated pattern based on the data from single-crystal X-ray analysis (Figure 7) shows good agreement between the two and thus reveals the crystalline purity of this compound. Small deviations in intensity and reflection position might be due to the fact that the powder measurement was done at room temperature in contrast to 190 K for the single-crystal measurement, and that the needle-like crystals preferably align in the capillary vertical to the beam.

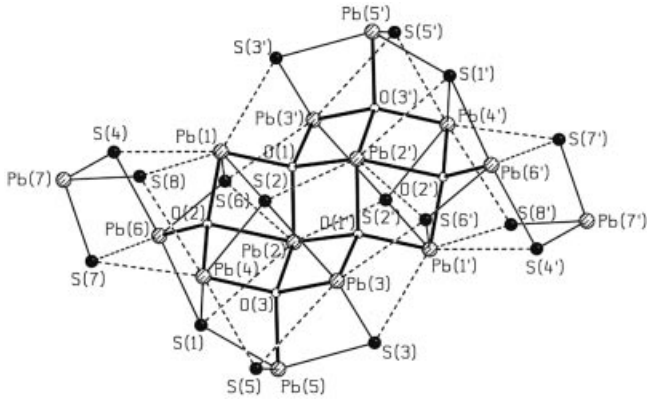

Figure 6. Molecular structure of $[Pb_{14}O_6\{S\text{-}2,6\text{-}(CH_3)_2C_6H_3\}_{16}]$ (**4**). C and H atoms omitted for clarity. Selected bond lengths [pm] (solid lines): Pb(1)–O(2) 225.0(10) Pb(1)–O(1) 231.9(9), Pb(2)–O(1) 227.2(9), Pb(2)–O(3) 238.6(9) Pb(2)–O(1′) 242.1(10) Pb(2)–O(2) 269.6(10), Pb(3)–O(1′) 229.8(8), Pb(3)–O(3) 232.0(10), Pb(1)–S(2) 285.0(4), Pb(4)–O(2) 226.8(9), Pb(4)–O(3) 228.2(9), Pb(5)–O(3) 229.5(9), Pb(6)–O(2) 221.5(10), Pb(3)–S(3) 285.9(5), Pb(4)–S(1) 302.4(5), Pb(4)–S(2) 305.5(4), Pb(5)–S(5) 264.6(5), Pb(5)–S(1) 289.8(6), Pb(5)–S(3) 289.9(6), Pb(6)–S(6) 274.4(5), Pb(6)–S(1) 293.5(5), Pb(6)–S(4) 299.8(5), Pb(7)–S(8) 262.7(6), Pb(7)–S(7) 263.1(6), Pb(7)–S(4) 270.4(6), Pb(7′)–S(8) 263.5(11), Pb(7′)–S(4) 264.1(9). Weak contacts [pm] (dashed lines): Pb(1)–S(4) 334.2, Pb(1)–S(6) 370.1, Pb(1)–S(8) 338.0, Pb(1)–S(3′) 323.2, Pb(2)–S(1) 361.1, Pb(2)–S(6) 333.6, Pb(2)–S(2′) 330.6, Pb(3)–S(5) 349.1, Pb(3)–S(6′) 325.0, Pb(4)–S(5) 331.2, Pb(4)–S(7) 338.6, Pb(4)–S(8) 370.0, Pb(6)–S(7) 322.8. Symmetry transformation for generation of equivalent atoms: $-x + 1$, $-y + 1$, $-z + 1$.

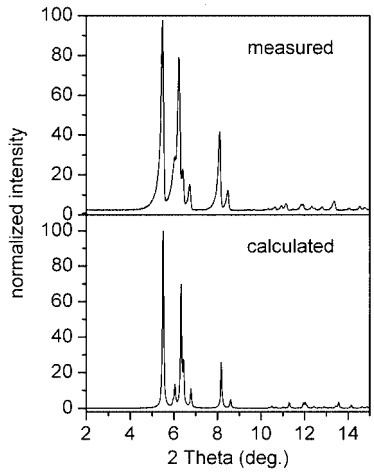

Figure 7. Measured (top) and calculated (bottom) powder diffraction pattern of $[Pb_{14}O_6\{S\text{-}2,6\text{-}(CH_3)_2C_6H_3\}_{16}]$ (**4**).

The UV/Vis spectra of **1**, **2**, and **4** in the solid state (Figure 8, bottom part) show a decrease in wavelength of the absorption onsets on going from **1** to **2** to **4**. Furthermore, the spectra display an almost featureless increase in absorbance down to 220 nm hardly indicating any maxima, of which the small shoulder at 430 nm (2.88 eV) in **4** is the most obvious. The solution spectrum of **4** is similar to that

of the ground crystalline powders. Starting from higher wavelengths one observes the first absorption maximum in solution as a broad shoulder at around 420 nm (2.95 eV; the extinction coefficient for **4** in THF at 420 nm is 1.63×10^5 M^{-1}cm^{-1}). The following increase in absorbance in the region from 420 nm to 310 nm indicates one further weakly resolved shoulder and shows a last maxima at 256 nm (4.84 eV). The onset of the absorption of **4** in the solid state is thus slightly shifted to higher wavelength, in agreement with findings in other solid-state spectra.[15] In contrast, for **1** the onset of the solution spectrum is shifted by roughly 100 nm compared to the solid-state spectrum, a fact which cannot be simply explained by influences of the different measurement techniques alone. Rather, we assume that oligomeric **1** dissociates in solution into smaller units, probably [Pb{S-2,6-$(CH_3)_2C_6H_3$}$_2$], which displays two absorption maxima at 333 nm (3.72 eV) and 258 nm (4.8 eV) with an extinction coefficient of 5.95×10^5 M^{-1}cm^{-1} at 333 nm. Solutions of **2** in THF decompose immediately after dissolution, as indicated by the formation of a dark precipitate, while the clear supernatant solution displays the same UV/Vis spectrum as measured for **1**. The powder diffraction pattern of the dark precipitate displays weak and broad peaks for cubic PbS[16,17] and weak but sharper ones for cubic elemental lead.[18] This suggests that **2** decomposes in THF to form PbS/Pb and [Pb{S-2,6-$(CH_3)_2C_6H_3$}$_2$].

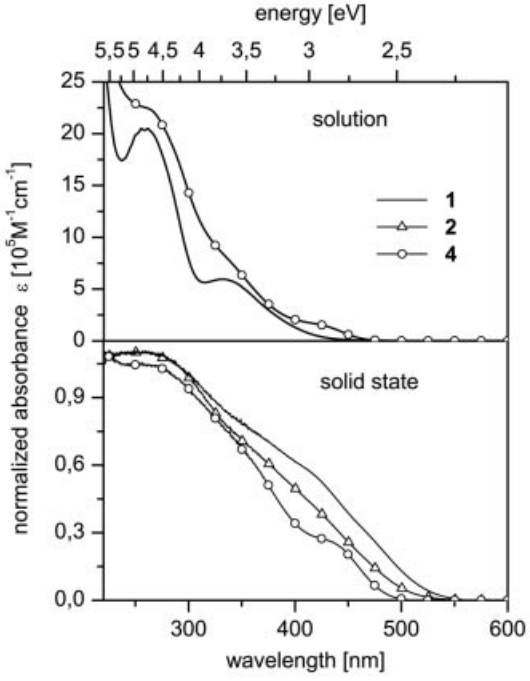

Figure 8. UV/Vis spectra of [Pb_{10}{S-2,6-$(CH_3)_2C_6H_3$}$_{20}$] (**1**), [Pb_6S{S-2,6-$(CH_3)_2C_6H_3$}$_{10}(C_4H_8O)_4$] (**2**), and [$Pb_{14}O_6${S-2,6-$(CH_3)_2C_6H_3$}$_{16}$] (**4**) in solution (THF) and the solid state (mull in nujol between two quartz plates).

These observations are currently part of further investigations where the effect of varying the reaction conditions (temperature, solvent, and stoichiometry) and the arenethiol are being studied. An additional focus will be the investigation of the reaction behavior of metal salts of the neighboring elements − tin, thallium and bismuth − with related thiols with a special focus on the formation of similar metal thiolate cluster complexes.

Experimental Section

General: Standard Schlenk techniques were employed throughout for the recrystallization of the preliminary reaction product using a double manifold vacuum line with high-purity dry nitrogen. All solvents were dried and distilled under nitrogen prior to use. Tetrahydrofuran and diethyl ether were dried with sodium/benzophenone, and pentane with $LiAlH_4$. $Pb(OOCCH_3)_2 \cdot 3H_2O$ (99+%) and 2,6-$(CH_3)_2C_6H_3$-SH (95%) were purchased from Aldrich. UV/Vis absorption spectra of cluster molecules in solution were measured with a Varian Cary 500 spectrophotometer in quartz cuvettes. Solid-state reflection spectra were measured for micron-sized crystalline powders between quartz plates with a Labsphere integrating sphere.

Synthesis: A hot solution (60 °C) of 2,6-$(CH_3)_2C_6H_3$SH (0.37 mL, 2.77 mmol) in 10 mL of ethanol was slowly added to a hot solution (60 °C) of $Pb(OOCCH_3)_2 \cdot 3H_2O$ (0.5 g, 1.32 mmol) in a mixture of 8 mL of C_2H_5OH and 2 mL of H_2O. A yellow precipitate was formed immediately which soon turned orange and finally became red. The reaction solution was heated at 60 °C for a further 30 min and then cooled to room temperature, filtered, washed with ethanol, and dried to give 0.49 g of an orange powder, which contained less sulfur than the expected product [Pb{S-2,6-$(CH_3)_2C_6H_3$}$_2$]. $C_{16}H_{18}PbS_2$ (481.64): calcd. C 39.9, H 3.8, S 13.31; found C 39.5, H 3.4, O 0.3, S 12.1.

1, 2, 3: For recrystallization the dried crude powder (0.49 g) was dissolved in 10 mL of THF and then layered with pentane by slow diffusion by evaporation from a connected flask to give a mixture of crystals of **1**, **2**, and **3**.

4: Pure crystals of **4** were obtained by dissolution of the crude powder (0.49 g) in 50 mL of THF and additional layering of this solution with pentane by slow diffusion by evaporation from a connected flask. (Yield: 0.063 g, 12.9% calculated for Pb). $C_{128}H_{144}O_6Pb_{14}S_{16}$ (5192.3): calcd. C 29.6, H 2.8, S 9.9; found C 29.9, H 2.6, S 10.2. Suitable crystals for X-ray analysis were obtained by careful layering of THF solutions of **4** with Et_2O in a Schlenk tube. The yield of **4** was increased by recrystallization of the crude powder (0.49 g) from 50 mL of THF in air without any layering with pentane. Yield: 0.29 g (56% calculated for Pb).

2: The solvents of the clear supernatant yellow solution from the crystallization of **4** were then removed in vacuo and the dry yellow-orange powder redissolved in 10 mL of THF. Layering of this solution with pentane by slow diffusion by evaporation from a connected flask yielded initially orange plate-like crystals of **2**, which tend to form solidified droplets of crystalline material during the layering process. After 2 d (ca. 6 mL of condensed pentane), the crystals were filtered and washed with pentane to yield 0.135 g (20.9% calculated for Pb) of **2**. $C_{96}H_{122}O_4Pb_6S_{11}$ (2935.9) (**2**·$4C_4H_8O$): calcd. C 39.3, H 4.2, S 12.1; found C 39.6, H 3.9, S 11.5.

1: The filtrate of **2** was again connected to the pentane flask and after 5 d yielded light-orange needles of **1**. Yield: 0.192 g (30.2% calculated for Pb). $C_{160}H_{180}Pb_{10}S_{20}$ (4816.3): calcd. C 39.9, H 3.8, S 13.3; found C 40.2, H 3.8, S 13.1. Continuation of the layering process resulted, at higher concentrations of condensed pentane, in the formation of a pale-yellow precipitate of unknown composition

Crystallographic Data: Data collection was carried out with a STOE IPDS II diffractometer equipped with a Schneider rotating anode using graphite-monochromated Mo-K_α (λ = 0.71073 Å) radiation at 190 K. The structure solutions and full-matrix least-squares refinements based on F^2 were performed with the SHELX-97 program package.[19] Molecular diagrams were prepared with the program SCHAKAL 97.[20]

1: Light-orange needle-like plates, 0.5 × 0.08 × 0.06 mm, M_r = 4816.14, orthorhombic, space group *Pbcn* (no. 60), a = 31.217(6), b = 21.294(4), c = 30.898(6) Å, V = 20539(7) Å^3, Z = 4, D_c = 1.558 g cm^{-3}, μ(Mo-K_α) = 8.405 mm^{-1} giving a final R_1 value of 0.0672 for 856 parameters and 11 336 unique reflections with $I \geq 2\sigma(I)$ and wR_2 of 0.1830 for all 15 896 reflections (R_{int} = 0.0771).

2: Orange hexagonal plates, 0.24 × 0.18 × 0.02 mm, M_r = 2935.74, triclinic, space group $P\bar{1}$ (no. 2), a = 13.965(3), b = 14.819(3), c = 15.670(3) Å, α = 94.47(3), β = 114.44(3), γ = 115.45°, V = 2533.5(9) Å^3, Z = 1, D_c = 1.924 g cm^{-3}, μ(Mo-K_α) = 10.206 mm^{-1} giving a final R_1 value of 0.0486 for 479 parameters and 8632 unique reflections with $I \geq 2\sigma(I)$ and wR_2 of 0.1424 for all 10 378 reflections (R_{int} = 0.0598).

3: Yellow triclinic blocks, 0.2 × 0.127 × 0.08 mm, M_r = 3480.27, triclinic, space group $P\bar{1}$ (no. 2), a = 14.637(3), b = 15.278(3), c = 15.491(3) Å, α = 97.20(3), β = 108.18(3), γ = 118.38(3)°, V = 2736.0(9) Å^3, Z = 1, D_c = 2.112 g cm^{-3}, μ(Mo-K_α) = 12.536 mm^{-1} giving a final R_1 value of 0.0556 for 552 parameters and 8149 unique reflections with $I \geq 2\sigma(I)$ and wR_2 of 0.1584 for all 10 265 reflections (R_{int} = 0.0602).

4: Yellow plate-like needles, 0.4 × 0.07 × 0.04 mm, M_r = 5192.05, triclinic, space group $P\bar{1}$ (no. 2), a = 15.948(3), b = 17.919(4), c = 18.273(4) Å, α = 109.42(3), β = 100.93(3), γ = 112.51(3)°, V = 4238.1(15) Å^3, Z = 1, D_c = 2.034 g cm^{-3}, μ(Mo-K_α) = 14.083 mm^{-1} giving a final R_1 value of 0.0840 for 428 parameters and 12 414 unique reflections with $I \geq 2\sigma(I)$ and wR_2 of 0.2377 for all 16 723 reflections (R_{int} = 0.0872).

CCDC-246835 (**1**), -246836 (**2**), -246837 (**3**) and -246838 (**4**) contain the supplementary crystallographic data for this paper. These data can be obtained free of charge from The Cambridge Crystallographic Data Centre via www.ccdc.cam.ac.uk/data_request/cif. X-ray powder diffraction patterns (XRD) were measured with a STOE STADI P diffractometer (Cu-K_α radiation, Germanium monochromator, Debye–Scherrer geometry) as a suspension of the crystals in sealed glass capillaries. Theoretical powder diffraction patterns were calculated on the basis of the atom coordinates obtained from single-crystal X-ray analysis by using the program package STOE WinXPOW.[21]

Acknowledgments

This work was supported by the Deutsch-Israelisches Programm (DIP) and the Deutsche Forschungsgemeinschaft (center for functional nanostructures CFN). The author is grateful to Prof. D. Fenske for helpful discussions and for providing excellent working conditions, E. Tröster for her invaluable assistance in the practical work, and Dr. Dale Cave for careful revision of the manuscript.

[1] E. Lifshitz, M. Bashouti, V. Kloper, A. Kigel, M. S. Eisen, S. Berger, *Nano Lett.* **2003**, *3*, 857–862.
[2] B. L. Wehrenberg, C. Wang, P. Guyot-Sionnest, *J. Phys. Chem. B* **2002**, *106*, 10 634–10 640.
[3] H. Du, C. Chen, R. Krishnan, T. D. Krauss, J. M. Harbold, F. W. Wise, M. G. Thomas, J. Silcox, *Nano Lett.* **2002**, *2*, 1321–1324.
[4] A. Olkhovets, R. C. Hsu, A. Lipovskii, F. W. Wise, *Phys. Rev. Lett.* **1998**, *81*, 3539–3542.
[5] S. Dehnen, A. Eichhöfer, D. Fenske, *Eur. J. Inorg. Chem.* **2002**, 279–317.
[6] A. Eichhöfer, P. Deglmann, *Eur. J. Inorg. Chem.* **2004**, 349–355.
[7] M. W. DeGroot, J. F. Corrigan, *J. Chem. Soc., Dalton Trans.* **2000**, 1235–1236.
[8] R. A. Shaw, M. Woods, *J. Chem. Soc. (A)* **1971**, 1569–1571.
[9] A. D. Rae, D. C. Craig, I. G. Dance, M. L. Scudder, P. A. Dean, M. A. Kmetic, N. C. Payne, J. J. Vittal, *Acta Crystallogr., Sect. B* **1997**, *53*, 457–465.
[10] B. Krebs, A. Brömmelhaus, B. Kersting, M. Niehaus, *Eur. J. Solid State, Inorg. Chem.* **1992**, *29*, 167–180 supplement.
[11] S. E. Appleton, G. G. Briand, A. Decken, A. S. Smith, *Dalton Trans.* **2004**, 3515–3520.
[12] P. B. Hitchcock, M. F. Lappert, B. J. Samways, E. L. Weinberg, *J. Chem. Soc., Chem. Commun.* **1983**, 1492–1494.
[13] F. T. Edelmann, J.-K. F. Buijink, S. A. Brooker, R. Herbst-Irmer, U. Kilimann, F. M. Bohnen, *Inorg. Chem.* **2000**, *39*, 6134–6135.
[14] A. F. Holleman, E. Wiberg, *Lehrbuch der Anorganischen Chemie*, 101st ed., Walter de Gruyter, Berlin, New York, **1995**, p. 977.
[15] A. Eichhöfer, O. Hampe, M. Blom, *Eur. J. Inorg. Chem.* **2003**, 1307–1314.
[16] H. E. Swanson, R. K. Fuyat, *National Bureau of Standards Circular* (U.S. Government Printing Office, Washington, D.C.), **1953**, vol. 539, p. 18.
[17] Y. Noda, K. Masumoto, S. Ohba, Y. Saito, K. Toriumi, Y. Iwata, I. Shibuya, *Acta Crystallogr., Sect. C* **1987**, *43*, 1443–1445.
[18] H. E. Swanson, E. Tatge, *National Bureau of Standards Circular* (U.S. Government Printing Office, Washington, D.C.), **1953**, vol. 539, p. 34.
[19] G. M. Sheldrick, *SHELX-97, Program for X-ray crystal structure determination and refinement*, University of Göttingen, Germany, **1997**.
[20] E. Keller, *SCHAKAL 97, A Computer Program for the Graphic Representation of Molecular and Crystallographic Models*, Universität Freiburg, Germany, **1997**.
[21] *STOE, WinXPOW*: STOE & Cie GmbH, Darmstadt, **2000**.

Received: August 6, 2004

